

Electronic Supplementary Information

Lithium-ion batteries with fluorinated mesogen-based liquid-crystalline electrolytes: molecular design towards enhancing oxidation stability

Shingo Takegawa,^a Kazuma Hamaguchi,^a Eiji Hosono,^b Shunsuke Sato,^c Go Watanabe,^{c,d,e} Junya Uchida^a and Takashi Kato^{*a,f}

^a Department of Chemistry and Biotechnology, School of Engineering, The University of Tokyo, 7-3-1 Hongo, Bunkyo-ku, Tokyo 113-8656, Japan

^b Global Zero Emission Research Center, National Institute of Advanced Industrial Science and Technology (AIST), 16-1 Onogawa, Tsukuba, Ibaraki 305-8569, Japan

^c Department of Physics, School of Science, Kitasato University, 1-15-1 Kitazato, Minami-ku, Sagami-hara, Kanagawa 252-0373, Japan

^d Department of Data Science, School of Frontier Engineering, Kitasato University, 1-15-1 Kitazato, Minami-ku, Sagami-hara, Kanagawa 252-0373, Japan

^e Kanagawa Institute of Industrial Science and Technology (KISTEC), 705-1 Shimoimaizumi, Ebina, Kanagawa 242-0435, Japan

^f Institute for Aqua Regeneration, Shinshu University, 4-17-1 Wakasato, Nagano 380-8553, Japan

*E-mail: kato@chiral.t.u-tokyo.ac.jp (T. Kato)

Table of contents:

1. Experimental methods -----	S2
2. Synthesis -----	S4
3. Liquid-crystalline properties of compound 1 -----	S7
4. Fourier transform infrared spectra -----	S9
5. Liquid-crystalline properties of complexes 1/LiTFSI -----	S10
6. Ionic conductivities -----	S12
7. Cyclic voltammograms -----	S13
8. Molecular dynamics simulations -----	S14
9. References -----	S19

1. Experimental methods

General procedures

All the reagents and solvents used for the synthesis of compound **1** were purchased from Tokyo Chemical Industry (Tokyo, Japan), FUJIFILM Wako Pure Chemical (Osaka, Japan), Sigma-Aldrich Japan (Tokyo, Japan), or Kanto Chemical (Tokyo, Japan) and they were used as received. All reactions were carried out under an argon atmosphere. Silica gel column chromatography was carried out using silica gel 60 from Kanto Chemical (spherical, 40–50 μm). Nuclear magnetic resonance (NMR) spectra were recorded on a JEOL JNM-ECX400 at 396 MHz for ^1H NMR and at 100 MHz for ^{13}C NMR in CDCl_3 . Chemical shifts of ^1H and ^{13}C NMR signals were quoted to internal standard $(\text{CH}_3)_4\text{Si}$ ($\delta = 0.00$) and CDCl_3 ($\delta = 77.00$), respectively, and expressed by chemical shifts in ppm (δ), multiplicity, coupling constant (Hz), and relative intensity. Matrix-assisted laser desorption ionization time-of-flight mass spectrometry (MALDI-TOF-MS) was carried out on a BRUKER autoflexTM speed spectrometer using dithranol or *trans*-2-[3-(4-*tert*-butylphenyl)-2-methyl-2-propenylidene]malononitrile as the matrix. Elemental analyses were performed on a CE-440 Elemental Analyzer (Exeter Analytical Inc.).

Preparation of the mixtures of **1** and LiTFSI

Lithium bis(trifluoromethanesulfonyl)imide (LiTFSI) in a lithium battery grade was purchased from Kishida Chemical (Osaka, Japan). The mixtures of compound **1** and LiTFSI were prepared by slow evaporation of the solvent at 80 °C from dry THF solutions containing requisite amounts of **1** and LiTFSI followed by drying under reduced pressure at 80 °C.

Characterization of liquid-crystalline properties

Polarized optical microscopy (POM) was performed with an Olympus BX51 polarizing optical microscope equipped with a Linkam 10084L hot-stage. Differential scanning calorimetry (DSC) was performed with a NETZSCH DSC 3500 Sirius system. X-ray diffraction (XRD) was performed with a Rigaku RINT-2500 diffractometer with a heating stage using a Ni-filtered $\text{CuK}\alpha$ radiation. Fourier transform infrared (FT-IR) spectra were recorded on a JASCO FT/IR-6100 Plus spectrometer and a JASCO IRT-5000 spectrometer with a Linkam 10084L hot-stage.

Ionic conductivity measurements

Ionic conductivities were measured by the alternating current impedance method with an impedance/gain-phase analyser (Solartron 1260, Hampshire, UK). The LC mixtures of compound **1** and LiTFSI were mounted on comb-shaped gold electrodes, which were covered with a glass plate with SiO_2 microparticle spacers (16 μm). Cole–Cole plots were obtained with an applied voltage of 0.1 V in the frequency range from 10 Hz to 1 MHz under temperature control with a Linkam 10013L hot-stage. Ionic conductivities were calculated to be the product of $1/R$ (Ω^{-1}) times cell constants (cm^{-1}) for comb-shaped gold electrodes, which were calibrated with the HI7033L 84 $\mu\text{S cm}^{-1}$ conductivity standard obtained from Hanna Instruments.

Cyclic voltammetry

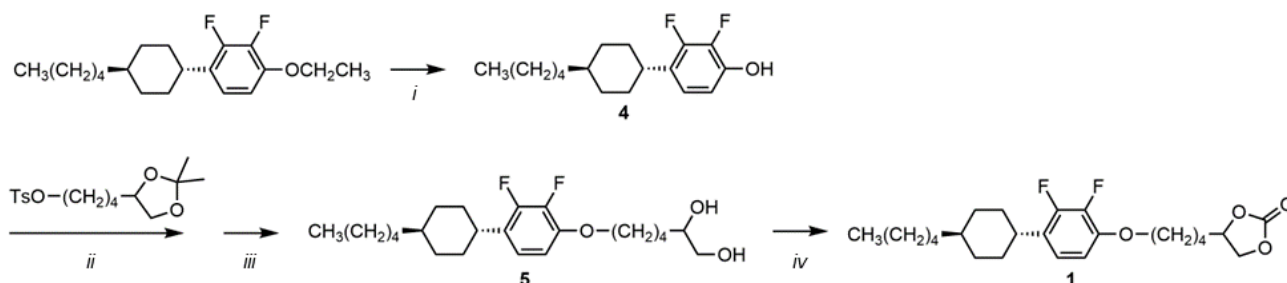
CR2032-type coin cells were assembled in an argon-filled glovebox using a stainless-steel plate (SUS316L) as the working electrode and lithium metal as the counter and reference electrodes. A porous polypropylene film with 25 μm thickness was used as a separator, which was filled with the LC electrolyte mixtures. The electrolytes were spread on the separators prior to the assembly of the cells. The assembled cells were placed in an oven at 110 $^{\circ}\text{C}$ for 15 min to allow the separators to soak up the LC electrolyte mixtures. Cyclic voltammograms were recorded with a Biologic VMP3 multichannel potentiostat (Vaucanson, France) within the potential range of -0.2 – 3.9 V, -0.2 – 4.3 V, and -0.2 – 5.0 V vs. Li/Li^+ at a scan rate of 0.05 mV s^{-1} at 60 $^{\circ}\text{C}$.

Charge–discharge experiments

The powder of LiFePO_4 (SLFP-PT30, Tianjin STL Energy Technology Co., Ltd., Tianjin, China) as the active material, carbon black (Super P-Li, Imerys Graphite & Carbon, Bironico, Switzerland) as a conductive additive, and poly(vinylidene difluoride) (PVDF#1300, Kureha Corporation, Tokyo, Japan) as a binder were mixed with in *N*-methyl-2-pyrrolidone with an ultrasonic homogenizer (UH-50, SMT Co., Ltd., Tokyo, Japan) to obtain the slurry of the electrode materials. The weight ratio of the solid materials was 65 : 30 : 5. The positive electrodes were prepared by spreading the slurries containing active materials onto an aluminium foil as a current collector, then dried at 100 $^{\circ}\text{C}$ in a vacuum oven over 90 min. The positive electrode was cut into disks with a diameter of 10 mm for the cell assembly. The thickness of the positive electrode on the Al current collector was estimated to be 10 μm^{S1} and the mass loading of the active material was 0.75 mg cm^{-2} . CR2032-type coin cells were assembled in an argon-filled glove box using prepared electrodes as a working electrode, lithium metal as negative and reference electrodes, and a porous polypropylene film with 25 μm thickness infiltrated with the LC electrolyte mixture as a separator. Galvanostatic charge–discharge curves of the electrode materials were recorded with a Hokuto Denko galvanostat in the potential range of 2.5 – 3.9 V vs. Li/Li^+ at the current density of 5 mA g^{-1} at 60 $^{\circ}\text{C}$. The specific current and capacity were calculated on the basis of the weight of the active materials.

2. Synthesis

Compound **1** was synthesized as shown in Scheme S1. 4-(2,2-dimethyl-1,3-dioxolan-4-yl)butyl *p*-toluenesulfonate was synthesized through the reported method.^{S2}



Scheme S1 Synthetic scheme of compound **1**. Reagents and conditions: (i) BBr₃, CH₂Cl₂; (ii) K₂CO₃, DMF; (iii) *p*-toluenesulfonic acid monohydrate, EtOH, H₂O; (iv) KF/Al₂O₃, diethyl carbonate.

2,3-Difluoro-4-(*trans*-4-pentylcyclohexyl)phenol (4**).** To a stirred solution of 1-ethoxy-2,3-difluoro-4-(*trans*-4-pentylcyclohexyl)benzene (5.36 g, 17.2 mmol) in dry CH₂Cl₂ (250 mL) was added BBr₃ in CH₂Cl₂ (1 mol L⁻¹, 25 mL, 25 mmol) at -78 °C dropwise slowly. The solution was warmed to room temperature and stirred for 25 h. The reaction was quenched by adding 2-propanol and water successively at 0 °C. The organic layer was separated and the aqueous layer was extracted with CH₂Cl₂. The combined organic layer was washed with brine, dried over anhydrous Na₂SO₄, filtered, and evaporated under reduced pressure. The residue was purified by using flash column chromatography (hexane/ethyl acetate = 90/10) and recrystallization from hexane to afford **4** as a white solid (4.15 g, 14.4 mmol, 85%).

¹H NMR (396 MHz, CDCl₃): δ = 6.85-6.81 (m, 1H), 6.70 (td, *J* = 8.3, 2.1 Hz, 1H), 5.01 (d, *J* = 4.1 Hz, 1H), 2.73 (tt, *J* = 12.2, 3.2 Hz, 1H), 1.87-1.81 (m, 4H), 1.43 (qd, *J* = 12.8, 3.3 Hz, 2H), 1.36-1.18 (m, 9H), 1.11-1.00 (m, 2H), 0.89 (t, *J* = 7.0 Hz, 3H).

¹³C NMR (100 MHz, CDCl₃): δ = 148.7 (dd, *J* = 245.6, 10.0 Hz), 142.4 (dd, *J* = 11.4, 1.9 Hz), 140.0 (dd, *J* = 238.4, 16.2 Hz), 128.0 (d, *J* = 12.4 Hz), 121.3 (t, *J* = 4.8 Hz), 111.6 (d, *J* = 2.9 Hz), 37.3 (s), 37.2 (s), 36.9 (s), 33.4 (s), 33.0 (s), 32.2 (s), 26.6 (s), 22.7 (s), 14.1 (s).

MS (MALDI-TOF): *m/z* calcd. for [M + H]⁺, 283.19; found: 284.08.

Elemental analysis: calcd. (%) for C₁₇H₂₄F₂O: C, 72.31; H, 8.57; found: C, 72.36; H, 8.75.

6-(2,3-Difluoro-4-(*trans*-4-pentylcyclohexyl)phenoxy)hexane-1,2-diol (5**).** A mixture of **4** (1.42 g, 5.02 mmol), 4-(2,2-dimethyl-1,3-dioxolan-4-yl)butyl *p*-toluenesulfonate (2.58 g, 7.86 mmol), and K₂CO₃ (1.40 g, 10.1 mmol) in dry DMF (30 mL) was stirred at 80 °C for 4.5 h. The mixture was poured into a saturated NH₄Cl aqueous solution and extracted with ethyl acetate twice. The combined organic layer was washed with brine three times, dried over anhydrous Na₂SO₄, filtered, and evaporated under reduced pressure. The residue was subjected to flash column chromatography (gradient from hexane/ethyl acetate = 100/0 to 90/10) to afford a colorless oil. The oil was successively dissolved in ethanol (containing 5% water, 100 mL). After the addition of *p*-toluenesulfonic acid

monohydrate (0.92 g, 4.8 mmol), the solution was stirred at 70 °C for 2 h. After evaporating the solvent under reduced pressure, the residue was dissolved in ethyl acetate and washed with a saturated NaHCO₃ aqueous solution and brine twice. The organic layer was dried over anhydrous Na₂SO₄, filtered, and evaporated under reduced pressure. The residue was purified by using flash column chromatography (hexane/ethyl acetate = 40/60) to afford **5** as a white solid (1.64 g, 4.12 mmol, 82% in 2 steps).

¹H NMR (396 MHz, CDCl₃): δ = 6.86-6.81 (m, 1H), 6.68-6.63 (m, 1H), 4.02 (t, *J* = 6.3 Hz, 2H), 3.79-3.74 (m, 1H), 3.72-3.66 (m, 1H), 3.49-3.43 (m, 1H), 2.77-2.71 (m, 1H), 2.06 (d, *J* = 4.1 Hz, 1H), 1.87-1.80 (m, 7H), 1.71-1.49 (m, 4H + water), 1.47-1.19 (m, 11H), 1.11-1.02 (m, 2H), 0.90 (q, *J* = 7.1 Hz, 3H).

¹³C NMR (100 MHz, CDCl₃): δ = 149.3 (dd, *J* = 245.1, 10.5 Hz), 146.1 (dd, *J* = 8.1, 2.4 Hz), 141.4 (dd, *J* = 246.0, 15.3 Hz), 128.4 (d, *J* = 12.4 Hz), 120.5 (t, *J* = 5.2 Hz), 109.4 (s), 72.1 (s), 69.6 (s), 66.7 (s), 37.3 (s), 37.2 (s), 36.9 (s), 33.4 (s), 33.0 (s), 32.7 (s), 32.2 (s), 29.1 (s), 26.6 (s), 22.7 (s), 22.0 (s), 14.1 (s).

MS (MALDI-TOF): calcd. for [M + Na]⁺, 421.25; found; 421.11.

Elemental analysis: calcd. (%) for C₂₃F₂H₃₆O₃: C, 69.32; H, 9.11; found: C, 69.30; H, 9.27.

4-(4-(2,3-Difluoro-4-(*trans*-4-pentylcyclohexyl)phenoxy)butyl)-1,3-dioxolan-2-one (1). A mixture of **5** (1.54 g, 3.86 mmol) and KF/Al₂O₃ (40wt%, 0.77 g) in diethyl carbonate (30 mL) was refluxed for 3.5 h. After cooling, the reaction mixture was diluted with dry CH₂Cl₂ and filtered. The filtrate was evaporated under reduced pressure. The residue was purified by using flash column chromatography (hexane/ethyl acetate = 70/30) and recrystallization from methanol to afford **1** as a white solid (1.19 g, 2.80 mmol, 73%).

¹H NMR (396 MHz, CDCl₃): δ = 6.87-6.82 (m, 1H), 6.67-6.63 (m, 1H), 4.75 (qd, *J* = 7.6, 5.0 Hz, 1H), 4.55 (t, *J* = 8.2 Hz, 1H), 4.09 (dd, *J* = 8.6, 7.2 Hz, 1H), 4.03 (t, *J* = 6.1 Hz, 2H), 2.77-2.71 (m, 1H), 1.89-1.85 (m, 10H), 1.48-1.19 (m, 11H), 1.11-1.01 (m, 2H), 0.89 (t, *J* = 7.0 Hz, 3H).

¹³C NMR (100 MHz, CDCl₃): δ = 154.9 (s), 149.3 (dd, *J* = 245.6, 10.0 Hz), 145.9 (dd, *J* = 8.1, 2.4 Hz), 141.4 (dd, *J* = 246.5, 15.7 Hz), 128.6 (d, *J* = 12.4 Hz), 120.5 (t, *J* = 5.2 Hz), 109.4 (d, *J* = 1.9 Hz), 76.8 (s), 69.3 (s), 69.3 (s), 37.3 (s), 37.2 (s), 36.9 (s), 33.6 (s), 33.4 (s), 33.0 (s), 32.2 (s), 28.6 (s), 26.6 (s), 22.7 (s), 21.3 (s), 14.1 (s).

MS (MALDI-TOF): calcd. for [M + Na]⁺, 447.23; found, 447.36.

Elemental analysis: calcd. (%) for C₂₄F₂H₃₄O₄: C, 67.90; H, 8.07; found: C, 67.82; H, 8.01.

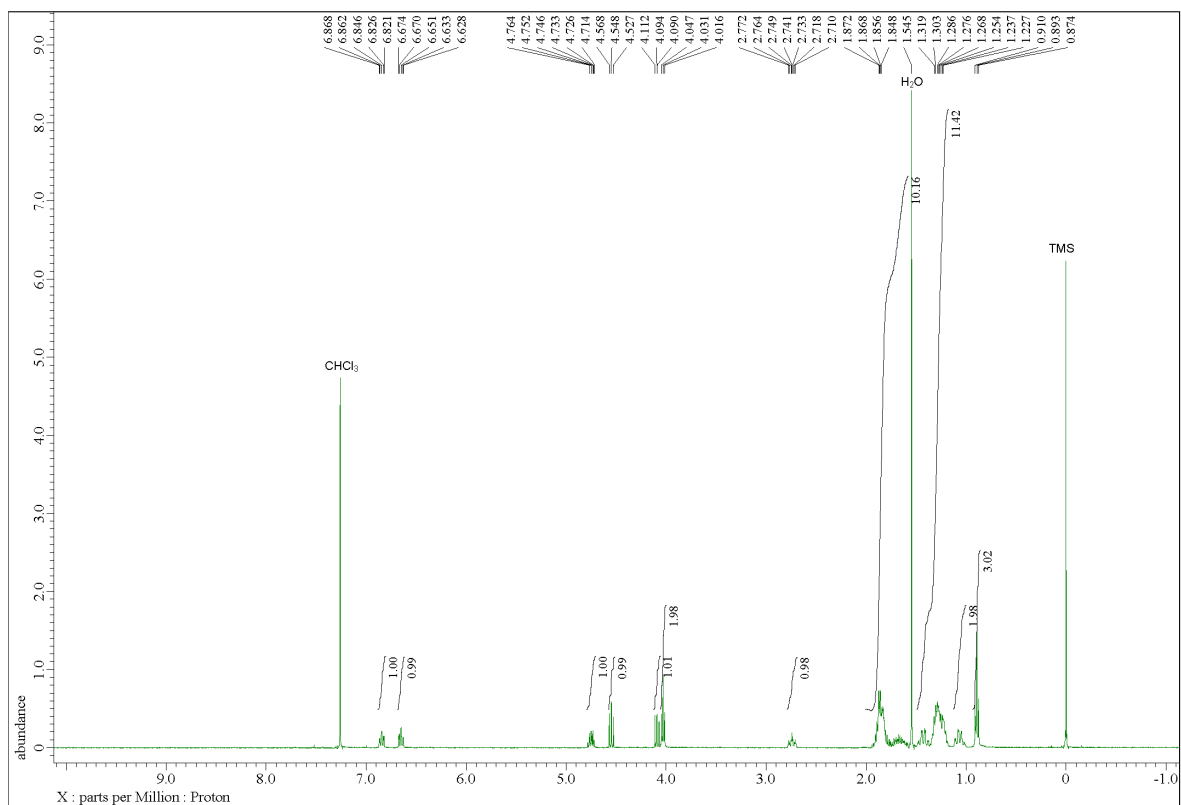


Fig. S1 ¹H NMR spectrum (396 MHz, CDCl₃) of compound 1.

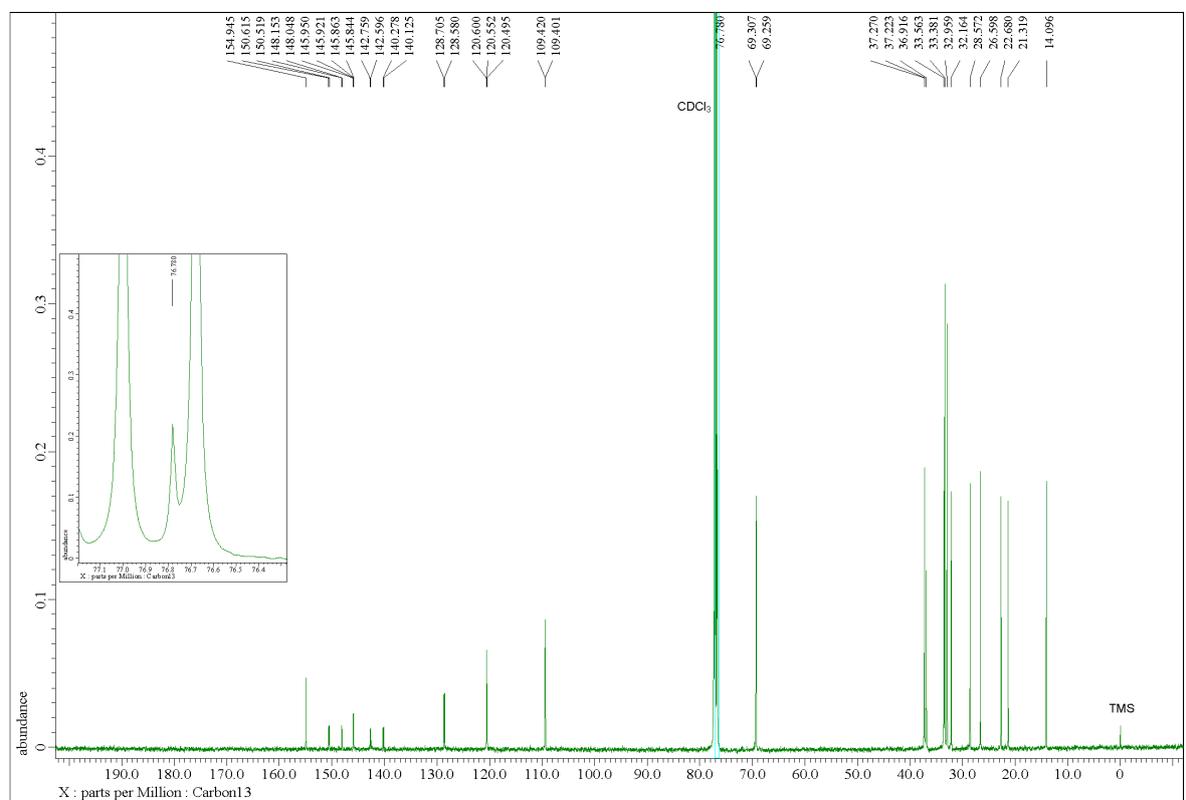


Fig. S2 ¹³C NMR spectrum (100 MHz, CDCl₃) of compound 1.

3. Liquid-crystalline properties of compound 1

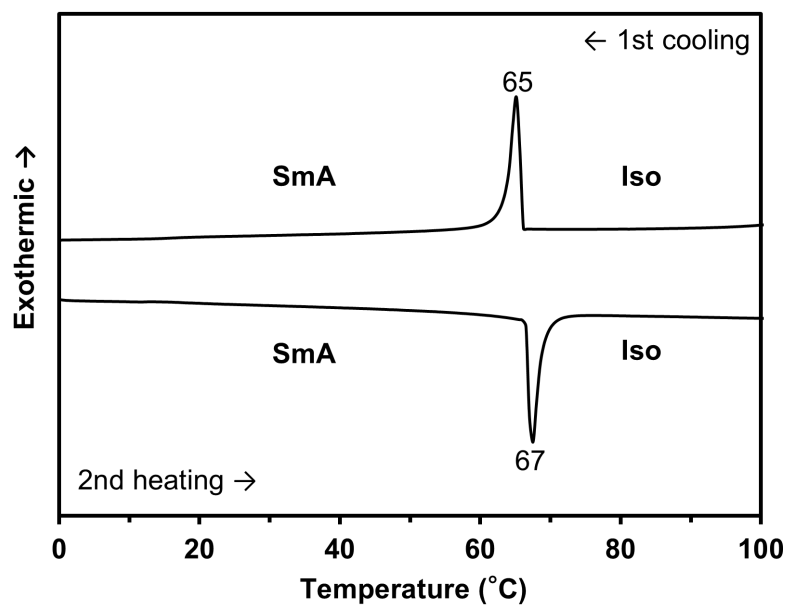


Fig. S3 DSC thermograms of compound 1 at a scanning rate of 10 K min⁻¹. Iso: isotropic; SmA: smectic A.

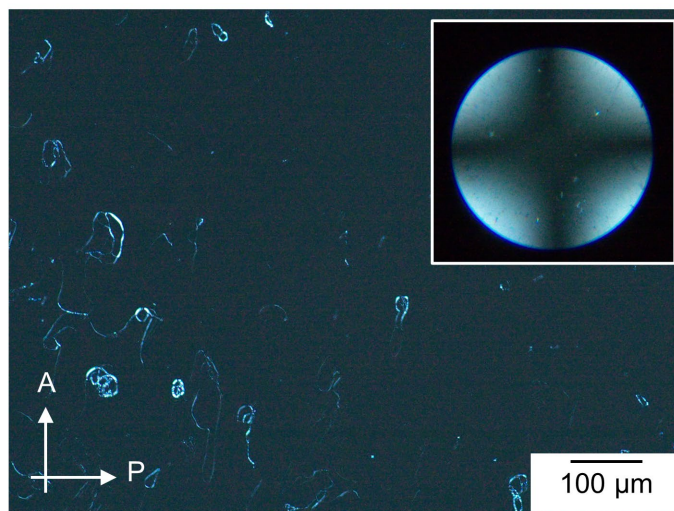


Fig. S4 POM image of compound 1 on glass substrates in the SmA phase at 25 °C. A: analyzer. P: polarizer. The inset shows the conoscopic image.

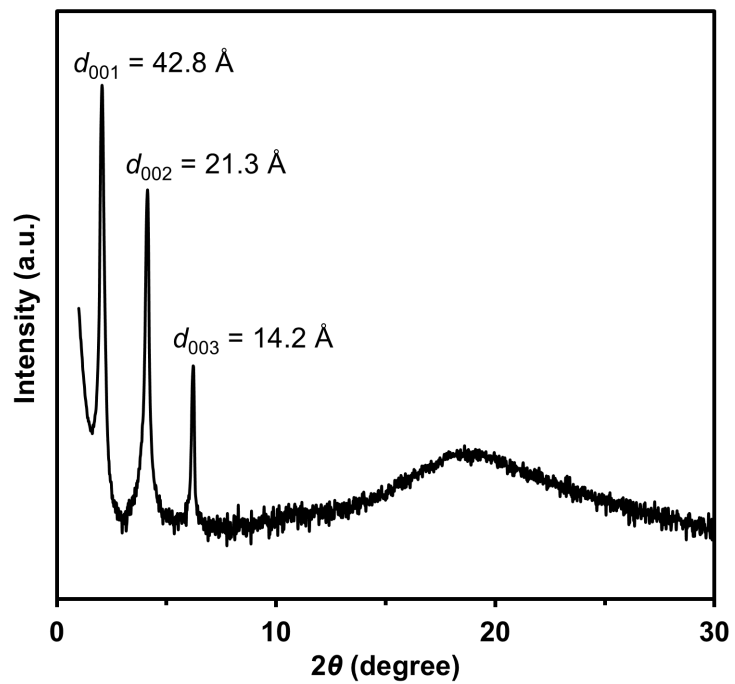


Fig. S5 XRD pattern of compound **1** in the SmA phase at 30 °C.

4. Fourier transform infrared spectra

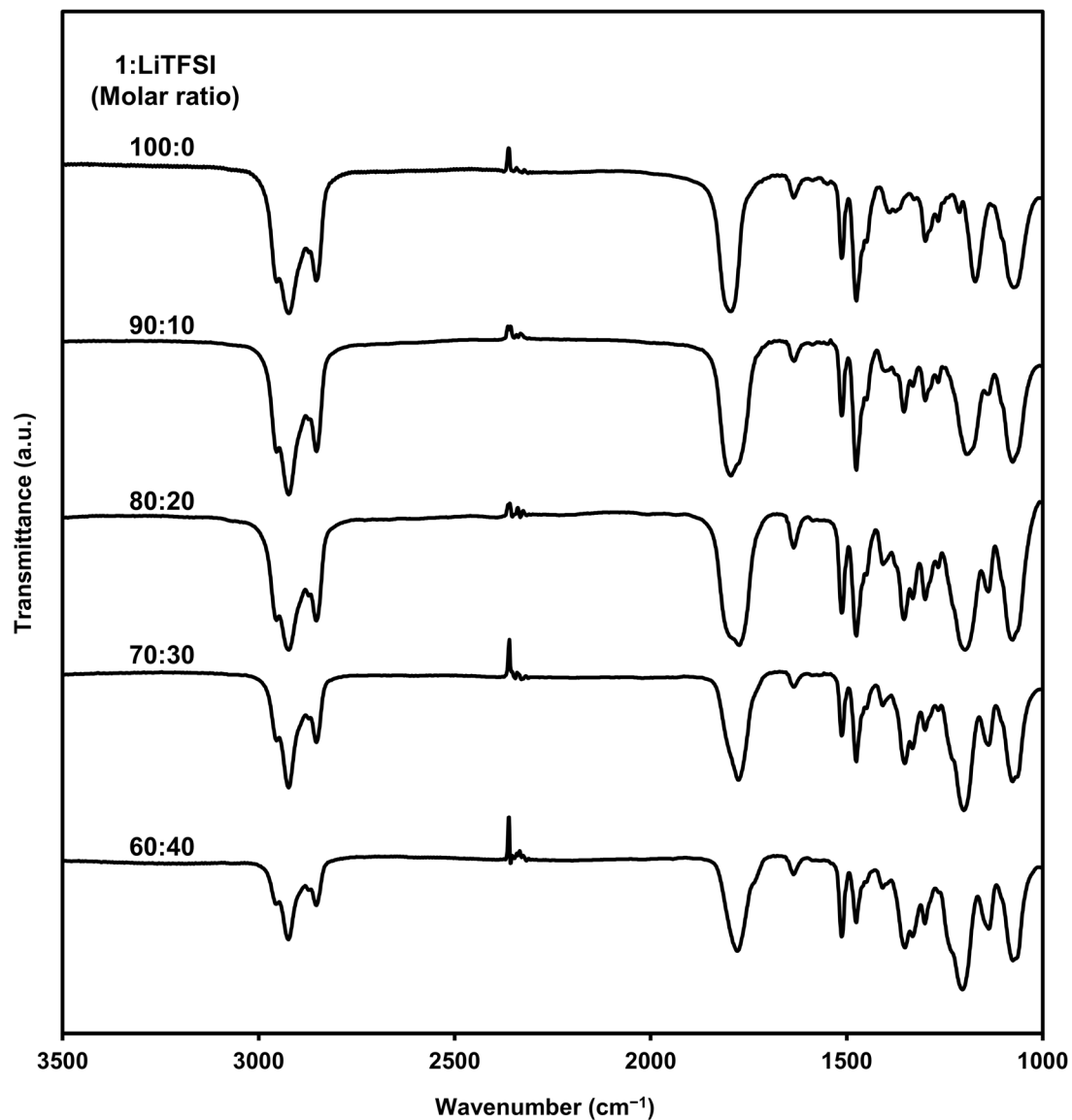


Fig. S6 FT-IR spectra of compound **1** and complexes **1**/LiTFSI in the SmA phases at 30 °C.

5. Liquid-crystalline properties of complexes 1/LiTFSI

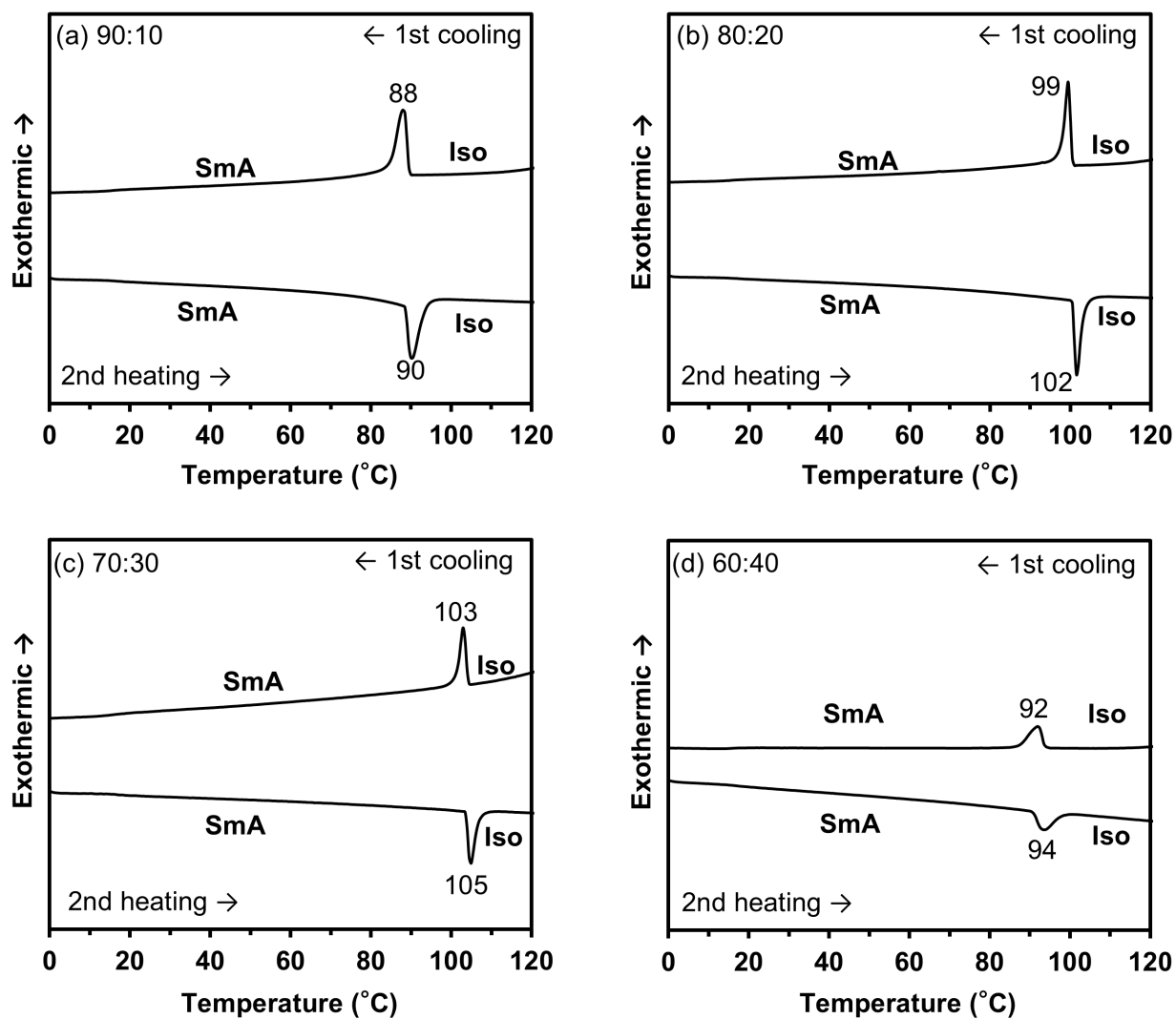


Fig. S7 DSC thermograms of complexes 1/LiTFSI in the (a) 90:10, (b) 80:20, (c) 70:30, and (d) 60:40 molar ratios at a scanning rate of 10 K min^{-1} . Iso: isotropic; SmA: smectic A.

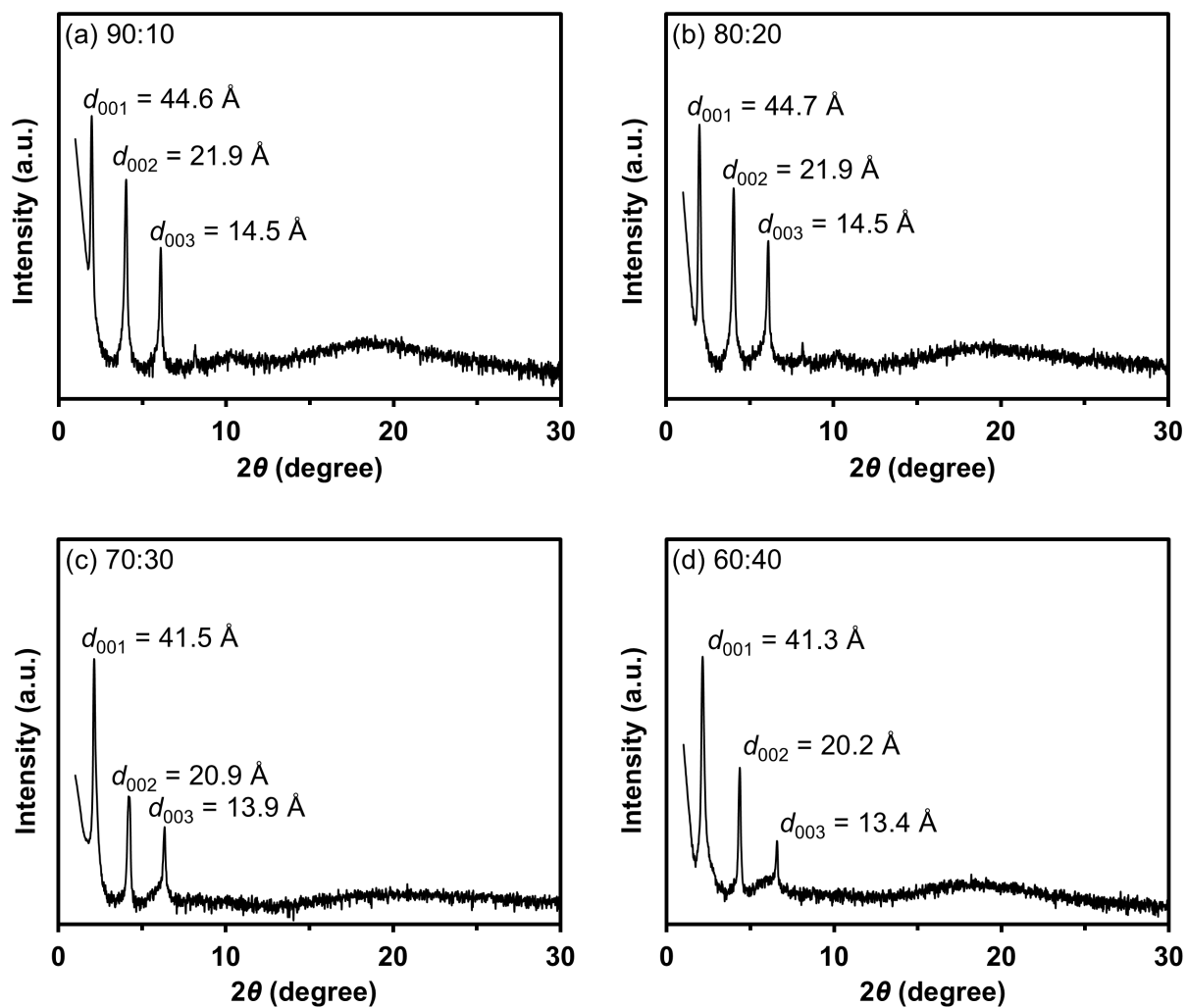


Fig. S8 XRD patterns of complexes **1**/LiTFSI in the molar ratios of (a) 90:10, (b) 80:20, (c) 70:30, and (d) 60:40 at 60 °C.

6. Ionic conductivities

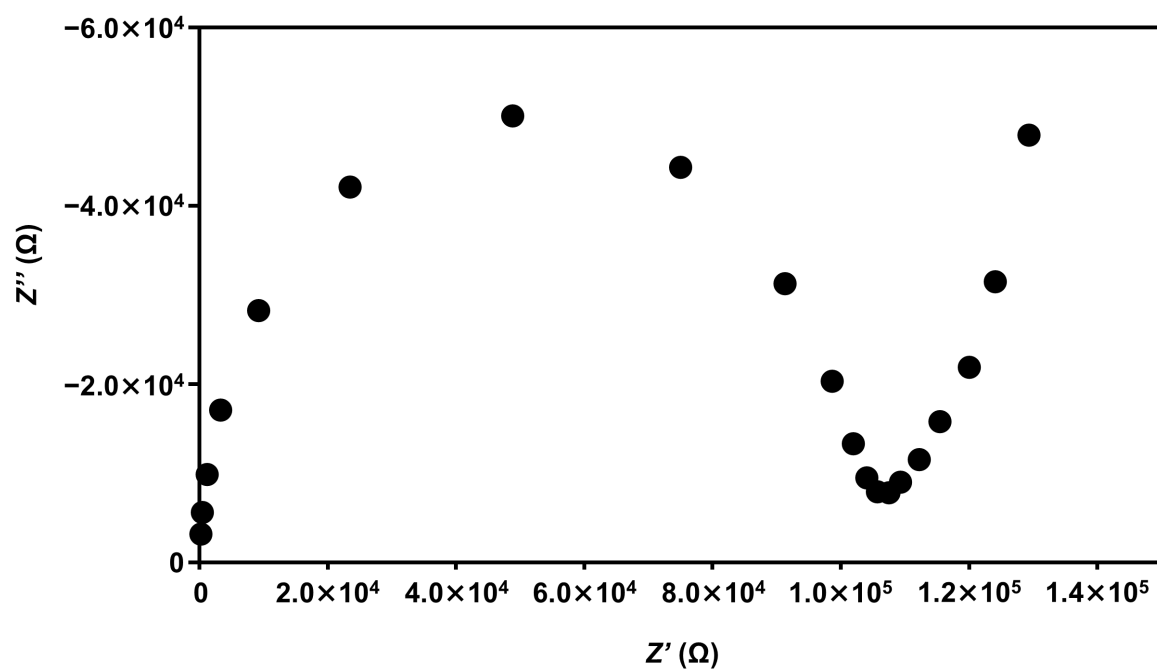


Fig. S9 Nyquist plots of 1/LiTFSI in the 80:20 molar ratio at 60 °C.

7. Cyclic voltammograms

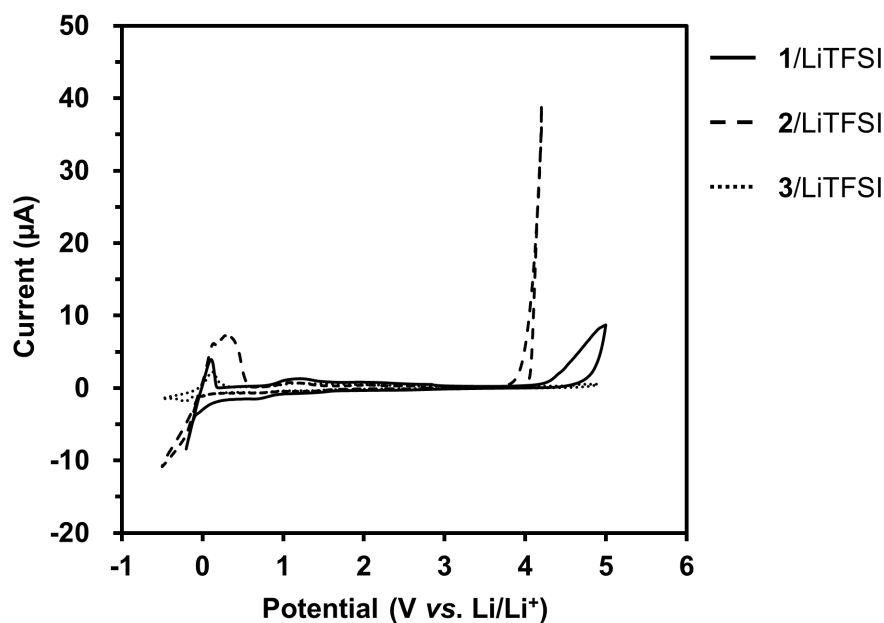


Fig. S10 Cyclic voltammograms of LC electrolytes **1**/LiTFSI in the 80:20 molar ratio (black solid line), **2**/LiTFSI in the 90:10 molar ratio^{S1} (black dashed line), and **3**/LiTFSI in the 80:20 molar ratio^{S1} (black dotted line) at 60 °C.

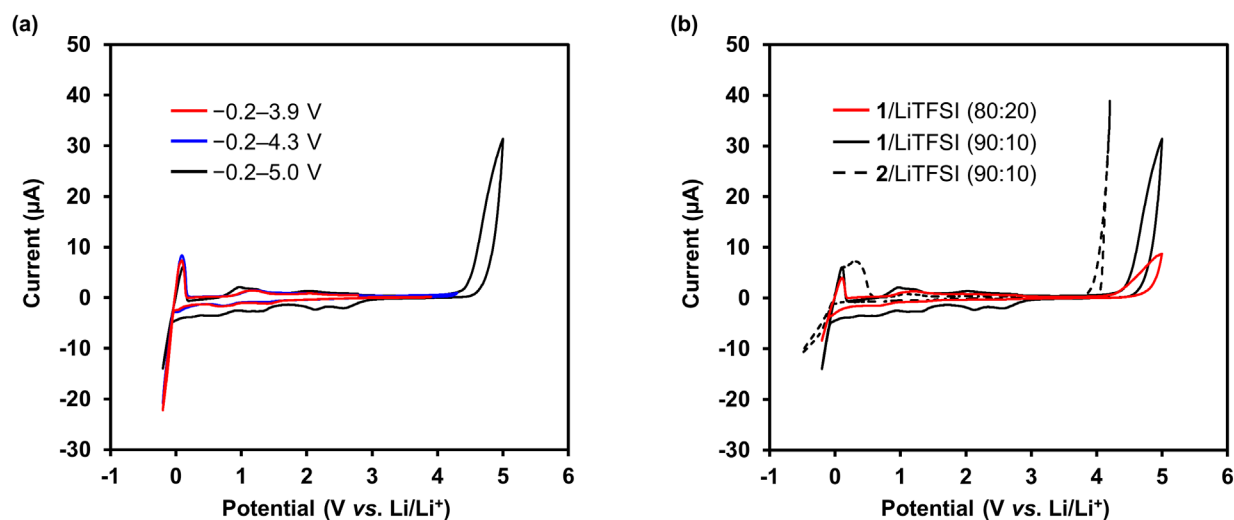


Fig. S11 Cyclic voltammograms of LC electrolytes at 60 °C. (a) **1**/LiTFSI in the 90:10 molar ratio in the voltage region of -0.2–3.9 V (red), -0.2–4.3 V (blue), and -0.2–5.0 V (black) vs. Li/Li⁺. (b) **1**/LiTFSI in the 80:20 molar ratio (red solid line), **1**/LiTFSI in the 90:10 molar ratio (black solid line), and **2**/LiTFSI in the 90:10 molar ratio^{S1} (black dashed line).

8. Molecular dynamics simulations

All-atom molecular dynamics (MD) simulations were performed using the MD program GROMACS 2016.3 and the models and methodologies followed our previous study^{S3}. Generalized Amber force field^{S4} parameters were used for calculating the intra- and intermolecular interactions. The partial atomic charges of the simulated molecule were calculated using the restrained electrostatic potential (RESP)^{S5} methodology, based on quantum chemical calculations using the B3LYP/6-31G(d,p) basis set by means of the GAUSSIAN 16 program.^{S6}

In this study, the pre-equilibration run of single periodic layer in the MD simulation box was initially carried out for 5 ns after the steepest energy minimization. For three layers obtained by stacking the single layer structure after the previous MD run, the pre-equilibration run of 5 ns and equilibration run of 500 ns were performed sequentially. Each layer was composed of 800 molecules and total number of molecules of three layers were 2400. In the initial structure, a pair of antiparallel molecules was placed on a square grid point in the xy plane. The area per molecule was set to 0.336 nm² for both compound **1** and **2**.

All MD simulations were performed under periodic boundary conditions with constant temperature and pressure. For the pre-equilibration run, the temperature and pressure of the system were kept constant by using the Berendsen thermostat and barostat^{S7} with relaxation times of 0.2 and 2.0 ps, respectively. The Nosé-Hoover thermostat^{S8} and the Parrinello-Rahman barostat^{S9} with relaxation times of 0.2 and 5.0 ps, respectively, were used for the equilibration run. The temperature of both the pre-equilibration and equilibration runs was set to 303 K. The time step was set to 2 fs since all the bonds connected to hydrogen atoms were constrained with the LINCS algorithm^{S10}. The smooth particle-mesh Ewald (PME) method^{S11} was employed to treat the long-range electrostatic interactions with a grid spacing of 0.30 nm. The real space cutoff for both the Coulomb and van der Waals interactions was 1.4 nm.

According to the previous study^{S12}, the two-dimensional radial distribution function (2D RDF) of the smectic layer was obtained by normalizing the number density of molecules present at distance r from molecule i by the average number density as follows:

$$g_{2D}(r) = \frac{1}{2\pi r \Delta r} \frac{A}{N} \frac{1}{N} \sum_{i=1}^N \Delta N_i(r)$$

where A is the area of the xy plane of the system, N is the number of molecules in the single layer, Δr is the thickness of the thin circle, and $\Delta N_i(r)$ is the number of molecules between the distance $r - \Delta r/2$ to $r + \Delta r/2$ with respect to molecule i . In this study, 2D RDF of the end carbon atom of the rigid rod core connected with the side alkyl chain was analyzed for the last 10 ns.

The orientational order parameter S was determined as the largest positive eigenvalue of tensor order parameter \mathbf{P} obtained from the following equation:

$$P_{\alpha\beta} = \frac{1}{N} \sum_{i=1}^N \frac{3}{2} n_{i\alpha} n_{i\beta} - \frac{1}{2} \delta_{\alpha\beta}$$

where n_i is normalized vector of the long axis of the specific group of the molecule, N is the total number of the molecules, and α, β is x, y, z . The orientational order parameters of the rigid core (S_C) and the alkyl spacer (S_a)

were calculated for the long axis vector connecting end atoms of each part.

Electron density profiles along the layer normal were analyzed by the method often used in the MD simulation studies for biomolecular systems.^{S13,S14}

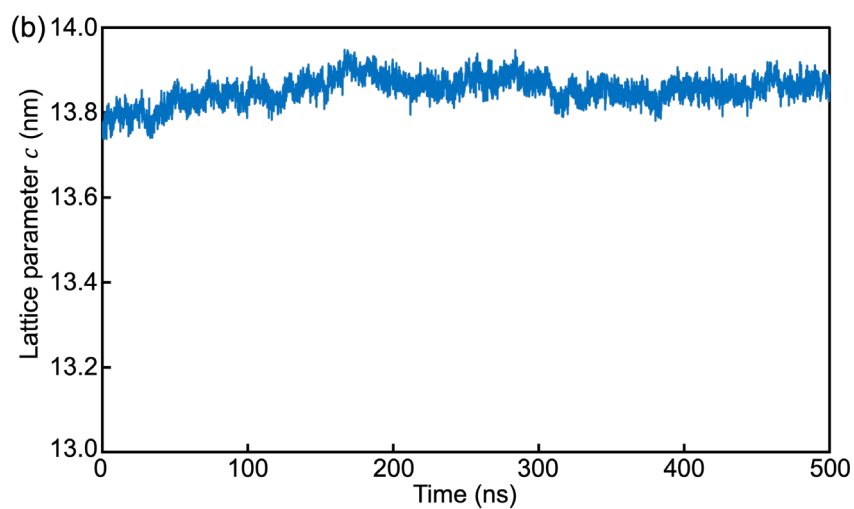
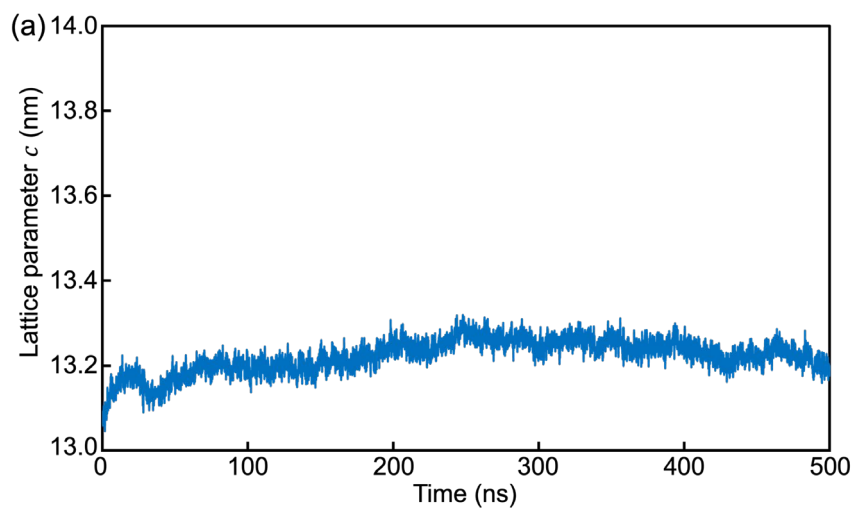


Fig. S12 Time dependences of lattice parameter (the c -axis) of rectangular MD simulation box: (a) compound **1** and (b) compound **2**.

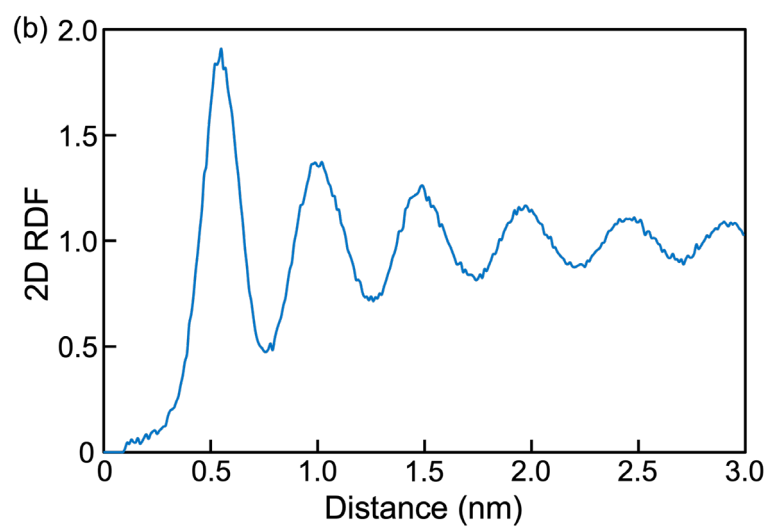
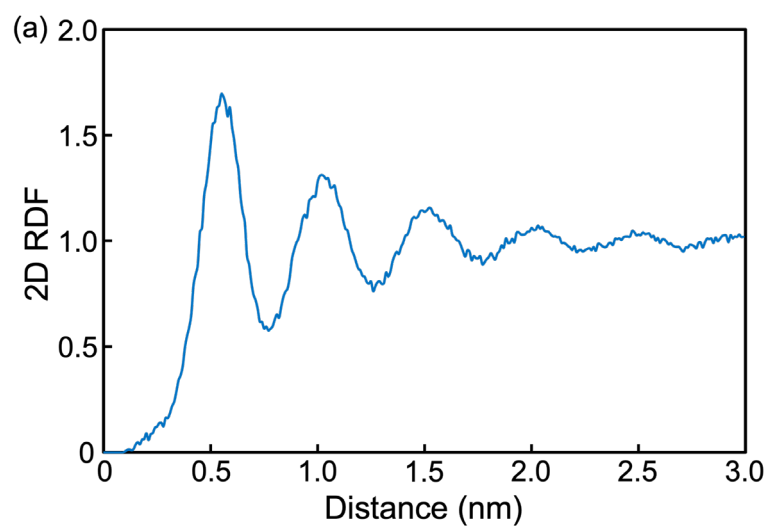


Fig. S13 2D RDFs for one representative layer: (a) compound **1** and (b) compound **2**.

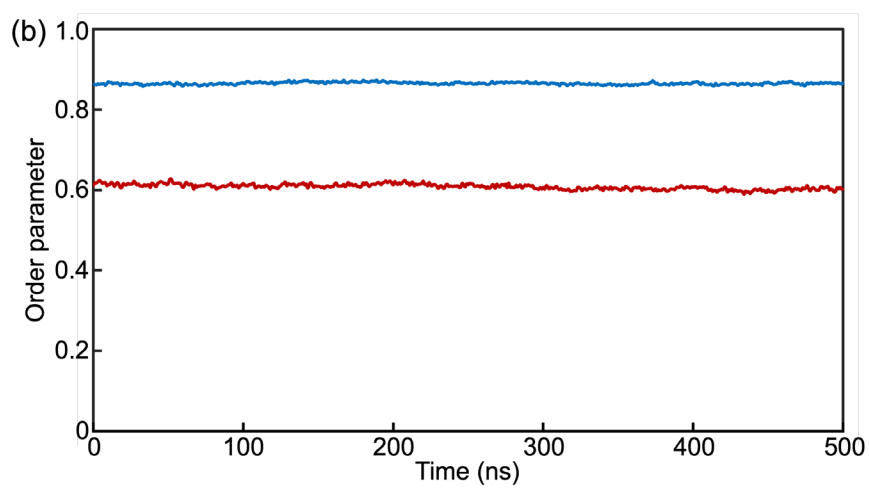
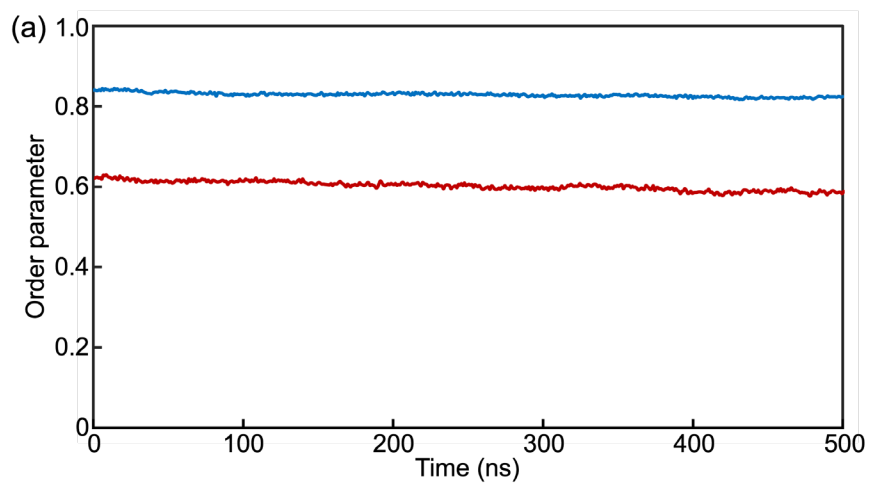


Fig. S14 Time dependences of order parameters of rigid core and alkyl spacer drawn with blue and red lines, respectively: (a) compound **1** and (b) compound **2**.

9. References

- S1. A. Kuwabara, M. Enomoto, E. Hosono, K. Hamaguchi, T. Onuma, S. Kajiyama and T. Kato, *Chem. Sci.*, 2020, **11**, 10631–10637.
- S2. S. P. Tanis and J. W. Raggon, *J. Org. Chem.*, 1987, **52**, 819–827.
- S3. K. Hamaguchi, H. Lu, S. Okamura, S. Kajiyama, J. Uchida, S. Sato, G. Watanabe, Y. Ishii, H. Washizu, G. Ungar and T. Kato, *ChemPhysChem*, 2023, **24**, e202200927.
- S4. J. Wang, R. M. Wolf, J. W. Caldwell, P. A. Kollman and D. A. Case, *J. Comput. Chem.*, 2004, **25**, 1157–1174.
- S5. I. Bayly, P. Cieplak, W. D. Cornell and P. A. Kollman, *J. Phys. Chem.*, 1993, **97**, 10269–10280.
- S6. M. J. Frisch, G. W. Trucks, H. B. Schlegel, G. E. Scuseria, M. A. Robb, J. R. Cheeseman, G. Scalmani, V. Barone, G. A. Petersson, H. Nakatsuji, X. Li, M. Caricato, A. Marenich, J. Bloino, B. G. Janesko, R. Gomperts, B. Mennucci, H. P. Hratchian, J. V. Ortiz, A. F. Izmaylov, J. L. Sonnenberg, D. Williams-Young, F. Ding, F. Lipparini, F. Egidi, J. Goings, B. Peng, A. Petrone, T. Henderson, D. Ranasinghe, V. G. Zakrzewski, J. Gao, N. Rega, G. Zheng, W. Liang, M. Hada, M. Ehara, K. Toyota, R. Fukuda, J. Hasegawa, M. Ishida, T. Nakajima, Y. Honda, O. Kitao, H. Nakai, T. Vreven, K. Throssell, J. A. Montgomery, Jr., J. E. Peralta, F. Ogliaro, M. Bearpark, J. J. Heyd, E. N. Brothers, K. N. Kudin, V. N. Staroverov, T. Keith, R. Kobayashi, J. Normand, K. Raghavachari, A. Rendell, J. C. Burant, S. S. Iyengar, J. Tomasi, M. Cossi, J. M. Millam, M. Klene, C. Adamo, R. Cammi, J. W. Ochterski, R. L. Martin, K. Morokuma, O. Farkas, J. B. Foresman and D. J. Fox, Gaussian 16, Revision C.01 (Gaussian, Inc., 2016).
- S7. H. J. C. Berendsen, J. P. M. Postma, W. F. van Gunsteren, A. DiNola and J. R. Haak, *J. Chem. Phys.*, 1984, **81**, 3684–3690.
- S8. S. Nosé, *Mol. Phys.*, 1984, **52**, 255–268.
- S9. M. Parrinello and A. Rahman, *J. Appl. Phys.*, 1981, **52**, 7182–7190.
- S10. B. Hess, H. Bekker, H. J. Berendsen and J. G. Fraaije, *J. Comput. Chem.*, 1997, **18**, 1463–1472.
- S11. T. Darden, D. York and L. Pedersen, *J. Chem. Phys.*, 1993, **98**, 10089–10092.
- S12. G. Watanabe, J. Saito, Y. Fujita and Y. Tabe, *J. Phys. Soc. Jpn.*, 2013, **82**, 084603–1/5.
- S13. R. W. Benz, F. Castro-Román, D. J. Tobias and S. H. White, *Biophys. J.*, 2005, **88**, 805–817.
- S14. S. Moradi, A. Nowroozi and M. Shahlaei, *RSC Adv.*, 2019, **9**, 4644–4658.